Suppression of perturbed free-induction decay and noise in experimental ultrafast pump-probe data

Patrick Nuernberger, Kevin F. Lee, Adeline Bonvalet, Thomas Polack, Marten H. Vos, Antigoni Alexandrou, Manuel Joffre

Suppression of perturbed free-induction decay and noise in experimental ultrafast pump–probe data

Patrick Nuernberger,[1,2] Kevin F. Lee,[1,2] Adeline Bonvalet,[1,2] Thomas Polack,[1,2] Marten H. Vos,[1,2] Antigoni Alexandrou,[1,2] and Manuel Joffre[1,2,*]

[1]*Laboratoire d'Optique et Biosciences, Ecole Polytechnique, CNRS*
[2]*Institut National de la Santé et de la Recherche Médicale, U696, 91128 Palaiseau, France*
[*]*Corresponding author: manuel.joffre@polytechnique.fr*

Received May 15, 2009; accepted September 4, 2009;
posted September 18, 2009 (Doc. ID 111455); published October 15, 2009

We apply a Fourier filtering technique for the global removal of coherent contributions, like perturbed free-induction decay, and noise, to experimental pump–probe spectra. A further filtering scheme gains access to spectra otherwise only recordable by scanning the probe's center frequency with adjustable spectral resolution. These methods cleanse pump–probe data and allow improved visualization and simpler analysis of the contained dynamics. We demonstrate these filters using visible pump/mid-infrared probe spectroscopy of ligand dissociation in carboxyhemoglobin. © 2009 Optical Society of America

OCIS codes: 320.7150, 300.6340, 190.4223.

Femtosecond pump–probe spectroscopy is a versatile tool to elucidate the initial dynamics of physical, chemical, and biological systems. Resolving the signal in both frequency and time is usually done to extract as much information as possible. This can be achieved using either scanning or multiplexing.

In the scanning approach, a probe pulse of duration Δt and moderate spectral width $\Delta\nu$ traverses the sample, and its pump-induced transmission change is measured as a function of the pump–probe delay τ. By repeating the experiment while scanning the probe center frequency ν_c, one obtains the two-dimensional (2D) pump–probe spectrum $\Delta T_s(\tau,\nu)$ (where ΔT indicates the difference in transmitted probe intensity). However, the spectrotemporal resolution is limited by the probe's time-bandwidth product $\Delta t\Delta\nu$, which is of the order of unity.

In the multiplexing approach, the order of probe frequency selection and the interaction is reversed—a broadband ultrashort probe is sent through the sample and then spectrally resolved in a spectrometer. This has two advantages: the acquisition time is considerably shorter, and no compromise between time and frequency resolution is needed, as they are set independently. However, $\Delta T_m(\tau,\nu)$ exhibits oscillations for $\tau<0$ in coherent systems where dephasing times are longer than the pulse duration [1–4]. This is from the perturbed free-induction decay (PFID, caused by the pump interacting with the probe-induced polarization) and the probe, which overlap and interfere after temporal stretching by the spectrometer. Although well understood, this effect results in counterintuitive pump–probe spectra.

In visible pump/IR probe spectroscopy, coherent contributions are generally evident in spectrally resolved data owing to long vibrational dephasing times T_2^v. For example, three recent publications [5–7] feature pronounced PFID and coherent spikes (a signal mainly due to cross-phase modulation (XPM) showing up while the pump and probe overlap temporally [8]) and state that data analysis starts from positive τ so that it is not perturbed by PFID or XPM. Hence, an approach to suppress these coherent contributions is desirable.

Such an approach has been recently developed theoretically, based on a 2D Fourier transform filtering scheme [9]. In this Letter, we demonstrate its applicability to visible pump/IR probe data and discuss its advantages and limitations. Our model system, ligand dissociation in carboxyhemoglobin (HbCO), was chosen for its narrow CO absorption band arising from the confining protein environment.

We use femtosecond pulses near 800 nm from a 1 kHz regenerative amplifier. A fraction is split off in front of the compressor, yielding positively chirped pulses ($\approx$120 ps). The other fraction is compressed and used to generate 400 nm pump pulses, which pass a continuously scanning delay stage and are chopped mechanically at 500 Hz, and 5.1 μm probe pulses [10,11]. Pump (pulse energy 0.4 μJ, focal diameter 140 μm) and probe (0.3 μJ, 60 μm) are individually focused and noncollinearly overlapped with parallel polarizations, resulting in an instrument response function (IRF) with a FWHM of 0.17 ps, found with a GaAs wafer. Our sample is 5 mM human hemoglobin in a D_2O [pD=7.6] Tris-HCl buffer, reduced with 40 mM dithionite under CO atmosphere, and 100 μm thick between CaF_2 windows. It is rotated so that the sample changes every laser shot. The transmitted probe is upconverted with the chirped 800 nm pulse [10,11] and recorded by a spectrometer with a 100×1340 pixel CCD camera. Individual spectra and motor positions are recorded for each laser shot. The spectra are binned to τ intervals of 30 fs, and a linear fit to the spectral baseline, excluding the absorption region, is subtracted. The average of all pump-blocked spectra serves as reference spectrum T used to convert between ΔT and $\Delta A=-\log_{10}(\Delta T/T+1)$ after filtering.

Figure 1(a) shows the multiplexed spectrum $\Delta T_m(\tau,\nu)$ obtained with a broadband probe. The pump dissociates the CO ligand from the heme, causing a transient bleaching of the A_1 band at $\approx$1951 cm^{-1} (ν_a=58.5 THz), which is nearly constant

during 1 ns [12]. There is also a small bleaching (less than 10% compared to the A_1 signal) that is due to the A_0 band at $\approx 1968\ \mathrm{cm}^{-1}$ (59.0 THz). The two structural substates correspond to two orientations of the distal histidine in the heme pocket, giving rise to two distinct absorption bands [13] of the Fe-bound CO.

Due to PFID, the increased transmission at ν_a does not set in at $\tau \approx 0$, but sets in over 1 ps earlier. Spectral oscillations are clearly visible for negative delays, producing characteristic hyperbolic lines associated with constant $\nu\tau$ values. For $\tau < 0$, the differential spectrum has spectral oscillations over the whole probe bandwidth, with a period of $1/\tau$. Conversely, at a given ν, the pump–probe signal quasi-periodically oscillates at frequency $|\nu - \nu_a|$ as a function of τ.

To suppress the oscillations, the data is transferred to shift space (ν_τ, t) by a 2D Fourier transform,

$$\widehat{\Delta T_m}(\nu_\tau, t) = \int\int \mathrm{d}\tau \mathrm{d}\nu \Delta T_m(\tau, \nu) e^{i(2\pi\tau\nu_\tau - 2\pi\nu t)}. \quad (1)$$

This data is multiplied by $i[\mathrm{sign}(t)+1]$ to enforce causality and by the complex filter function

$$\hat{f}(\nu_\tau, t) = \exp[-|2\pi\nu_\tau t|/2 + i(2\pi\nu_\tau t)/2], \quad (2)$$

motivated by the fact that the spectrotemporal resolution is limited by the probe, which in shift space reads

$$\hat{\mathcal{E}}(\nu_\tau, t) = \exp\left[-\frac{(2\pi\nu_\tau)^2 \Delta t^2}{16 \ln 2} - \frac{t^2 \ln 2}{\Delta t^2} + \frac{i(2\pi\nu_\tau t)}{2}\right]. \quad (3)$$

The $1/e^2$ width of $|\hat{\mathcal{E}}(\nu_\tau, t)|$ for any transform-limited (TL) pulse of duration Δt lies within the $1/e^2$ width of $|\hat{f}(\nu_\tau, t)|$. Hence, the filter damps away contributions located at $|2\pi\nu_\tau t| > 4$ (the filter's $1/e^2$ limit), as they cannot be due to dynamics probed by any TL pulse in the scanning approach. See [9] for the detailed theory. The filtered data is then Fourier transformed back to (τ, ν) space, and the imaginary part $\Delta T_f(\tau, \nu)$ is further analyzed. In the filtered data of Fig. 1(b), the oscillations are completely removed. Only a cross-shaped structure remains, owing to PFID contributions that change too slowly with frequency (along $\tau = 0$) or delay (along $\nu = \nu_a$) to be filtered out. Hence, unwanted coherent signals can be considerably suppressed, permitting a more straightforward visualization of the data. Note that neither the IRF nor the actual duration of the probe (which should be nearly TL and not have a very structured spectrum) are explicitly considered for this filtering method.

We confirmed good filtering with simulated data: a homogeneously broadened four-level system with two levels, both in an electronic ground and excited state described by Bloch equations; and pulse durations 120 fs, i.e., IRF FWHM 0.17 ps, $T_2^v = 1.15$ ps, $T_2^e = 40$ fs, and infinite population lifetimes. Pump and probe intensities are adjusted to allow a comparison of simulation and experiment (Fig. 1), which agree excellently even though neither inhomogeneity, the weak A_0 absorption, the finite sample thickness, nor XPM are considered.

If spectral features do not all start at the same delay (e.g., in coherent control with complex pump pulses), PFID cannot be simply ignored by cutting negative delays and can obscure interesting data. To demonstrate this, we simulated a simple scenario with an adjacent absorption line instantaneously bleached 4 ps after the first (Fig. 2). Perturbations

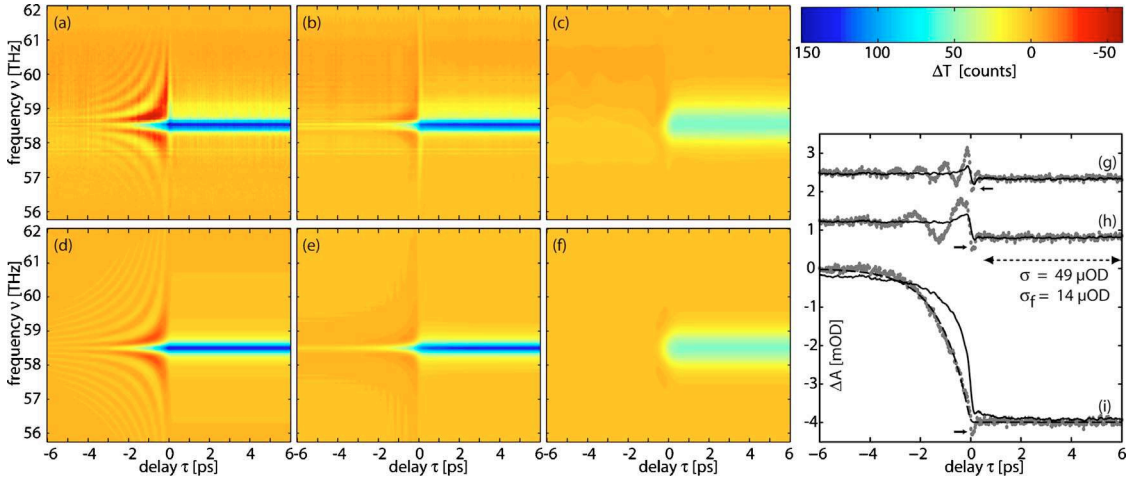

Fig. 1. (Color online) Left, application of the Fourier filtering technique to experimental data (top row) and simulated data (bottom row). (a) 400 nm pump/5.1 μm probe spectrally resolved $\Delta T_m(\tau, \nu)$ data of HbCO; (b) filtered data $\Delta T_f(\tau, \nu)$ using filter (2) as described in the text; (c) filtered data using Eq. (3) as filter to emulate $\Delta T_s(\tau, \nu)$ that would be obtained in the scanning approach with a 600 fs probe pulse. The evolution of $\Delta T_s(\tau, \nu)$ for probe durations from 300 fs to 2 ps is available as a movie (Media 1). (d)–(f) Simulations corresponding to (a)–(c). Right, transient absorption signals at (g) 59.6 THz, (h) 59.0 THz (A_0 band), and (i) 58.5 THz (A_1 band) before (dots) and after (line) the filtering procedure; (g) and (h) are vertically offset by 2.4 and 1.2 mOD for clarity. In (h), the standard deviation before (σ) and after (σ_f) filtering is given for the indicated interval 0.5 ps $< \tau <$ 6 ps; (i) includes a fit (dashed line) to a single exponential convolved with the IRF. The arrows mark a small coherent spike that is also reduced after filtering.

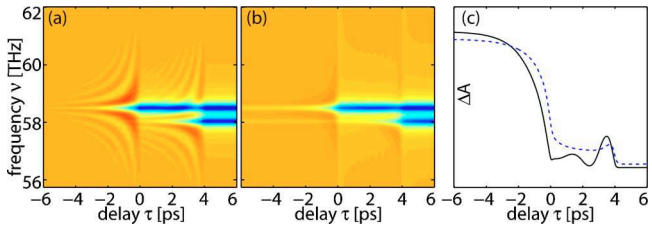

Fig. 2. (Color online) Simulation with two lines at 58.5 and 58.0 THz bleached at $\tau=0$ and 4 ps, respectively, (a) before and (b) after filtering. Transient absorption at 58.5 THz is shown in (c) before (solid) and after (dashed) filtering.

to the signal of the first line are mostly removed by filtering, which also qualitatively reveals the step at 4 ps owing to a population contribution from the adjacent line.

We further demonstrate another useful filter technique with our experimental data—a pump–probe spectrum $\Delta T_s(\tau,\nu)$ obtained with the scanning method can also be calculated from $\Delta T_m(\tau,\nu)$, provided the latter is measured with a short-enough probe pulse [9]. We achieve this with the same procedure, but with (3) rather than (2) as the filter. Figure 1(c) has results for $\Delta t=600$ fs. The oscillations are entirely removed, whereas the spectral resolution is degraded owing to the time-bandwidth product of the emulated probe. The asymmetry in Fig. 1(c) is due to the A_0 band. The advantage of this method is that it combines the short acquisition time of multiplexing with a produced pump–probe spectrum whose interpretation is straightforward. Despite a compromise between time and frequency resolutions, these parameters can be set *after* the experiment, as demonstrated in Media 1. Note that the relation between ΔT_s and ΔT_m resembles that between pulse representations in optics, like the Husimi and Wigner distributions (e.g., [14]); the first is a 2D convolution of the second with, e.g., a Gaussian function. Interestingly, the Husimi (as ΔT_s) is more intuitive than the Wigner (as ΔT_m), at the cost of the spectrotemporal resolution. In a way, the filtered function ΔT_f is the best attempt to combine the advantages of both.

While the filtering is done in ΔT, an analysis of molecular properties is performed in ΔA, to avoid effects from the probe's spectral intensity. As an example, three traces are shown in Figs. 1(g)–1(i). On resonance [Fig. 1(i)], the PFID leads to an exponential decay for $\tau<0$ [2,4]. A fit yields a constant of 1.15 ps, which would correspond to a Lorentzian of 9.2 cm^{-1} FWHM (reported inhomogeneous linewidth 8 cm^{-1} [15], Gaussian fit to our data 8.3 cm^{-1}). After filtering, the transient absorption at ν_a is more intuitive—only a small feature from the cross-shaped PFID remainder can be observed before the almost unaffected population signal sets in at $\tau=0$. This is also the case for the signals at $\nu\neq\nu_a$ [Figs. 1(g) and 1(h)]: the expected oscillations for $\tau<0$ have disappeared after filtering.

When multiplied with the filter function, components of $\Delta\hat{T}_m(\nu_\tau,t)$ far from the shift space axes are efficiently damped, as is white noise spanning the entire shift space. This efficient noise reduction is evident in Fig. 1(h), where the standard deviation of the A_0 population signal decreases by 70%. Finally, a reduction of the coherent spike can be clearly observed as well (arrows in Fig. 1).

In conclusion, the use of femtosecond pulses, which are shorter than the characteristic dephasing times of the system under study, leads to oscillations in pump–probe spectra that may obscure the analysis and extraction of characteristic dynamics. With a simple and general Fourier filtering scheme that is independent of the actual pulse durations, we demonstrated that these coherent signals can be mostly removed. Also, experimental noise is efficiently reduced, while the population dynamics remain virtually unaltered. In a different scheme with the field representation as the filter, scanning approach spectra with adjustable spectral resolution can be obtained from a single spectrally resolved measurement. The versatile pump–probe data procured with the different filters can be used to better visualize and more easily analyze the underlying molecular processes, which is especially beneficial for complex systems where an adequate theoretical model is not available.

We thank Agence Nationale de la Recherche (ANR-BLAN-0286) and Deutsche Akademie der Naturforscher Leopoldina (BMBF-LPDS 2009-6) for support.

References

1. B. Fluegel, N. Peyghambarian, G. Olbright, M. Lindberg, S. W. Koch, M. Joffre, D. Hulin, A. Migus, and A. Antonetti, Phys. Rev. Lett. **59**, 2588 (1987).
2. C. H. Brito Cruz, J. P. Gordon, P. C. Becker, R. L. Fork, and C. V. Shank, IEEE J. Quantum Electron. **24**, 261 (1988).
3. M. Joffre, D. Hulin, A. Migus, A. Antonetti, C. Benoit à la Guillaume, N. Peyghambarian, M. Lindberg, and S. W. Koch, Opt. Lett. **13**, 276 (1988).
4. P. Hamm, Chem. Phys. **200**, 415 (1995).
5. K. Neumann, M.-K. Verhoefen, I. Weber, C. Glaubitz, and J. Wachtveitl, Biophys. J. **94**, 4796 (2008).
6. C. Schumann, R. Groß, M. M. N. Wolf, R. Diller, N. Michael, and T. Lamparter, Biophys. J. **94**, 3189 (2008).
7. D. Wolpert, M. Schade, and T. Brixner, J. Chem. Phys. **129**, 094504 (2008).
8. M. Lorenc, M. Ziolek, R. Naskrecki, J. Karolczak, J. Kubicki, and A. Maciejewski, Appl. Phys. B **74**, 19 (2002).
9. T. Polack, Opt. Express **14**, 5823 (2006).
10. K. J. Kubarych, M. Joffre, A. Moore, N. Belabas, and D. M. Jonas, Opt. Lett. **30**, 1228 (2005).
11. J. Treuffet, K. J. Kubarych, J.-C. Lambry, E. Pilet, J.-B. Masson, J.-L. Martin, M. H. Vos, M. Joffre, and A. Alexandrou, Proc. Natl. Acad. Sci. USA **104**, 15705 (2007).
12. P. A. Anfinrud, C. Han, and R. M. Hochstrasser, Proc. Natl. Acad. Sci. USA **86**, 8387 (1989).
13. I. J. Finkelstein, A. M. Massari, and M. D. Fayer, Biophys. J. **92**, 3652 (2007).
14. S. Fechner, F. Dimler, T. Brixner, G. Gerber, and D. J. Tannor, Opt. Express **15**, 15387 (2007).
15. M. D. Fayer, Annu. Rev. Phys. Chem. **52**, 315 (2001).